Zaytoun *et al. Afr J Urol* (2021) 27:61
https://doi.org/10.1186/s12301-021-00165-7

African Journal of Urology

ORIGINAL RESEARCH Open Access

Role of non-contrast magnetic resonance imaging in pre-surgical evaluation of renal masses in renal impairment patients

Osama M. Zaytoun[1*], Reda M. Darweesh[2], Salma A. Gaber[2] and Rafik M. Ibrahim[2]

Abstract

Background: The aim of this work is to study the role of non-contrast MRI in pre-surgical evaluation of renal masses in renal impairment patients as confirmed by both intraoperative and histopathological findings. Intraoperative and histopathological findings were correlated with radiological data.

Methods: This prospective study included 20 patients comprising 25 renal masses. The data were collected in a period from April 2018 to September 2019. All patients underwent partial or radical nephrectomy by the same surgeon.

Results: Based on MRI findings, 9 masses (36%) and 8 masses (32%) were found to be associated with collecting system invasion and perinephric fat invasion, respectively. Histopathological assessment confirmed only 6 cases (24%) with collecting system invasion and 7 cases (28%) demonstrated perinephric fat. Seven masses (28%) had intralesional hemorrhage detected by MRI and confirmed by pathological findings. The MRI detected 6 cases (24%) with lymph nodes invasion, while the histopathological assessment confirmed lymphatic invasion in 7 cases (28%). Only 2 cases (8%) had vascular invasion detected by preoperative MRI and confirmed by histopathology and surgery. The final histopathological examination confirmed 20 malignant neoplasms (80%: RCC = 18, leiomyosarcoma = 2), 3 benign neoplasms (12%: angiomyolipoma = 1, oncocytoma = 2) and 2 non-neoplastic benign masses (8%: renal abscess = 1, xanthogranulomatous pyelonephritis = 1).

Conclusion: Non-contrast MRI is a crucial imaging tool in renal impairment patients who cannot be examined with contrast-enhanced CT or MRI. It assesses the extent of the renal sinus fat and the perinephric fat invasion.

1 Background

Recently, as a result of increased use of high-resolution cross-sectional imaging, the number of incidentally discovered solid renal masses has increased, requiring more imaging characterization for proper diagnosis [1]. This characterization extends beyond the simple determination of malignancy and benignity, as it determines and guides the therapeutic approach and follow-up management [2].

In addition to enabling proper characterization of solid renal lesions, cross-sectional imaging is also necessary for staging purposes in patients with known disease, for assessment of recurrence in patients with previously treated disease, and for active surveillance in high-risk patients [3].

RCC is one of the most frequently diagnosed adult cancers, accounting for 2–3% of all adult malignancies [4]. There are two main benign lesions that may be difficult to differentiate from RCC. These are angiomyolipoma (AMLs), in particular the lipid-poor subtype, and oncocytoma, which represent 3–7% of all renal tumors [5].

Because of the heterogeneity of imaging features as well as overlapping imaging characteristics of renal masses,

*Correspondence: ozaytoun@gmail.com
[1] Department of Urology, Faculty of Medicine, University of Alexandria, Alexandria, Egypt
Full list of author information is available at the end of the article

identifying reliable imaging criteria for recognition of malignant versus benign masses remains a challenging task. Several imaging parameters have been proposed to distinguish the different renal lesions. Abdominal ultrasonography and computed tomography (CT) are commonly used for a variety of renal indications. MR imaging can be particularly helpful when renal lesions are detected [6].

Traditionally, patients with impaired renal function could not be imaged with a CT scan with iodinated contrast media (ICM) due to the risk of contrast-induced nephropathy (CIN). These patients were alternatively imaged by MRI with gadolinium. However, the recent identification of the association between nephrogenic systemic fibrosis (NSF) and gadolinium administration has created significant challenges for radiologists when faced with the need for evaluation with contrast-enhanced cross-sectional imaging. As a result, the use of non-contrast MRI is thought to be the solution for renal impairment patients [4]. The aim of this work is to study the role of non-contrast MRI in pre-surgical evaluation of renal masses in renal impairment patients.

2 Methods

The study included 20 patients with renal impairment presenting with renal mass detected by ultrasonography or non-contrast CT and referred our institute for non-contrast MRI evaluation before surgical intervention (partial or radical nephrectomy) performed in the urology department.

The medical ethics were considered including informed consent that was obtained from all cases included in the study after explaining the purpose of the study. Confidentiality was maintained throughout the study.

Initial routine evaluation included thorough history, clinical examination and serum creatinine and eGFR assessment. Operative data were obtained and correlated with the radiological data. Histopathological analysis for the surgical specimens obtained for all patients and correlated with the radiological data and considered as the reference gold standard.

3 MR Imaging protocol

MRI sequences were acquired on Ingenia 3Tesla closed magnet MRI machine (Philips Medical systems, Netherlands), as well as Ingenia 1.5Tesla closed magnet MRI machine (Philips Medical systems, Eindhoven, The Netherlands). The choice of either machine was entirely based on availability, and comparison between the results of each was beyond the scope of this study. Axial T1-weighted, axial and coronal T2-weighted images as well as axial diffusion-weighted images were acquired, and apparent diffusion coefficient (ADC) maps were reconstructed on the work station.

4 MRI acquisition protocols, sequences and parameters used

a. Turbo spin-echo T2-weighted sequence (TSE): TR 1100/TE 80, flip angle 90°, field of view 200(±20), matrix size 320 × 299, slice thickness 3 mm and gap between slices 3 mm.
b. Turbo spin-echo T1-weighted sequences (TSE): TR 525/TE 16, flip angle 90°, matrix size 368 × 242, slice thickness 3.5 mm and gap used between slices 3.5 mm.
c. Diffusion-weighted sequences (DWI): TR 1632/TE 72, matrix 108 × 105, field of view 370(±20), slice thickness 3.5 mm with gap between slices 3.5 mm and 3 different b values were used (0,500,1000 s/mm^2) in all patients.
d. ADC maps were reconstructed on the workstation for qualitative and quantitative assessment of DWI images. The lowest mean ADC value was obtained after measuring the ADC value in different areas. The ROI is fitted in a homogenous solid area averaging about 0.5 cm^2 (could be changed in size depending on size of the lesion). ADC value was measured in the malignant area.

5 Results

The study included 20 patients with a total number of 25 renal masses (3 patients had bilateral renal masses and 2 patients had two masses in the same kidney). The surgical intervention encompassed 13 radical nephrectomy and 10 partial nephrectomy. All surgeries were performed by the same surgeon in the urology department. Table 1 shows the final histopathological diagnosis of the renal masses included in the study.

6 Non-contrast magnetic resonance imaging (MRI) findings and correlation with surgical and pathological findings

1 *Distribution of the renal mass*
Figure 1 summarizes the distribution and location of renal masses as evaluated by preoperative non-contrast MRI.
2 *Composition of the mass and presence of intralesional hemorrhage and necrosis*
Eleven lesions were seen entirely solid (44%), 3 cystic lesions (12%), and eleven solid lesions with necrotic areas (44%) (Fig. 2) (Table 2).

Table 1 Distribution of lesions based on their final histopathological diagnosis ($n=25$)

Distribution of lesions based on their final histopathological diagnosis	No	Percentage
Malignant neoplasms	20	80.0%
Renal cell carcinoma	18/20	90.0%
Clear cell RCC	8/18	44.0%
Papillary RCC	5/18	28.0%
Chromophobe RCC	2/18	11.0%
Multiseptated cystic RCC	1/18	5.0%
Mixed clear cell and papillary features	1/18	5.0%
Carcinoma of collecting duct of Bellini	1/18	5.0%
Leiomyosarcoma	2/20	10.0%
Benign neoplasms	3	12.0%
Angiomyolipoma	1	4.0%
Oncocytoma	2	8.0%
Non-neoplastic benign masses (Infective process)	2	8.0%
Renal abscess	1	4.0%
Xanthogranulomatous pyelonephritis	1	4.0%
Total	25	100.0%

Among the 25 masses, 7 (28%) masses showed intralesional hemorrhage detected by MRI and confirmed by pathological findings (Table 3) (Fig. 3a). Masses with hemorrhagic content are detected in the MRI as areas of hyperintensity in T1-weighted images.

3 *Assessment of invasion of renal sinus fat and collecting system*

Out of 8 masses found to have renal sinus fat invasion on preoperative MRI (Fig. 2), surgical findings confirmed only 6 of them (24%) and the pathological findings stated that only 5 cases (20%) had renal sinus fat invasion (Table 4).

Preoperative MRI showed that 9 masses had collecting system invasion: out of those only 7 and 6 cases were confirmed by surgical and pathological finding, respectively (Table 4).

4 *Assessment of invasion of renal capsule and perinephric space*

Surgical and pathological data confirmed the presence of renal capsule and perinephric fat invasion in 7 cases out of 8 cases was initially spotted on MRI (Fig. 2). (Table 4).

5 *Invasion of the lymph-vascular space*

Six cases were found to have enlarged para-aortic lymph nodes on MRI (Fig. 2 b, c). However, the surgical and the pathological findings confirmed seven cases to be associated with enlarged para-aortic lymph nodes (2: reactive lymphoid hyperplasia, 5: lymphatic metastasis) (Table 4).

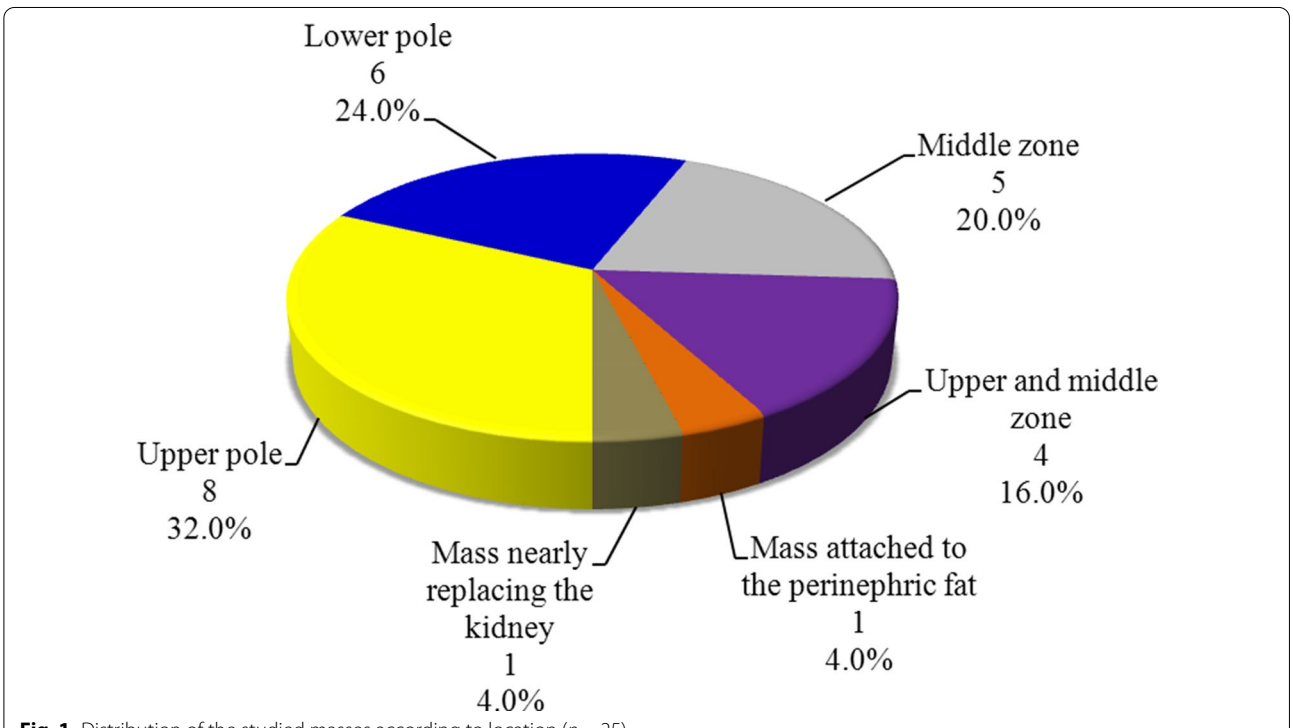

Fig. 1 Distribution of the studied masses according to location ($n=25$)

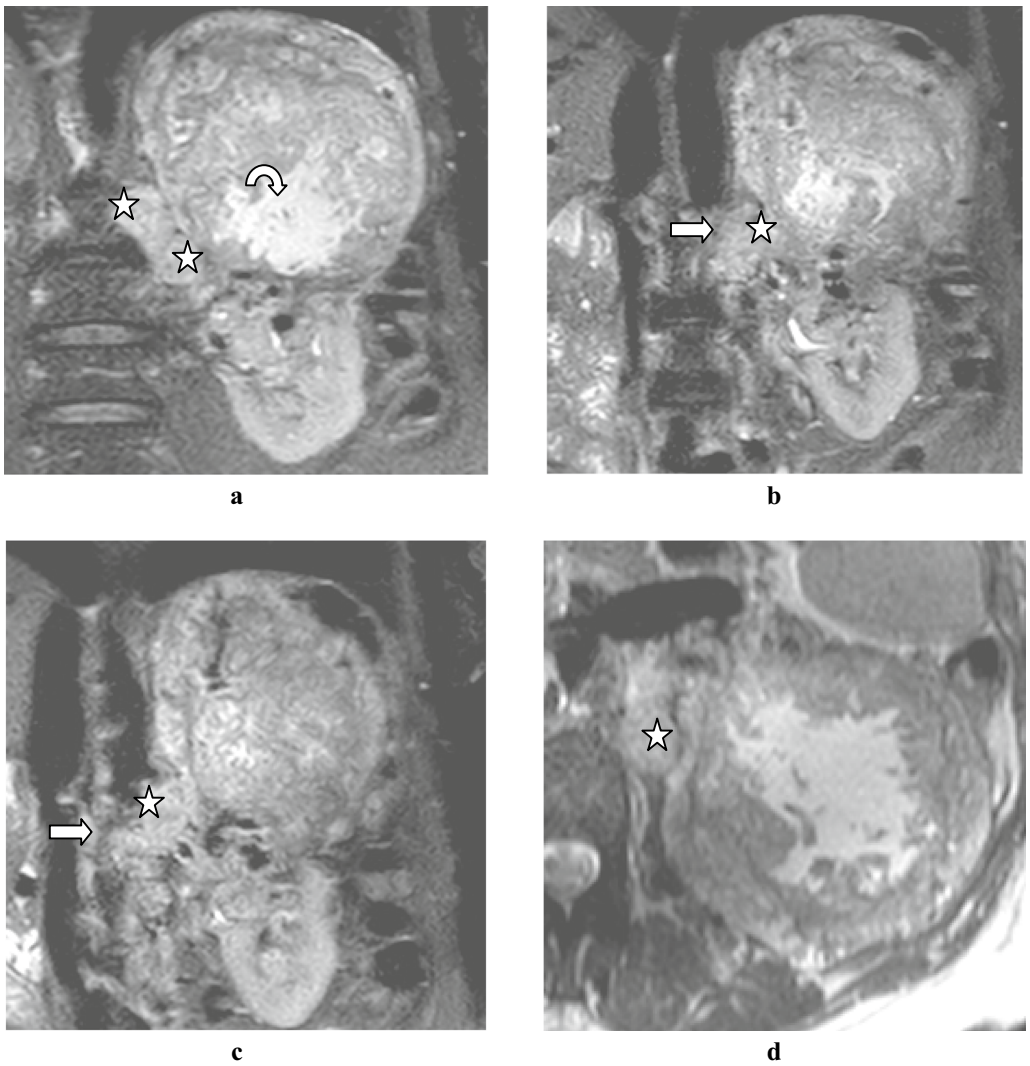

Fig. 2 Coronal T2w images with fat suppression (SPAIR) **a**, **b**, **c** and axial T2w fat suppression (SPAIR) image **d**, showing partially exophytic heterogeneous focal lesion arising from the upper pole of the left kidney, with T1 hypo- and T2 hyperintense areas, a central area of hyperintensity seen representing central necrotic area (curved arrow). The tumor tissue is seen reaching renal hilum with extension into the renal sinus fat, invasion of the upper and middle calyceal system of the left kidney with invasion of the renal capsule and extension into the perinephric fat, the tumor tissue is seen inseparable from the spleen. Multiple pathologically enlarged regional lymph nodes (white stars). A hyperintense soft tissue extension of the tumor is seen expanding the left renal vein reaching end of the vein into the IVC, still clear IVC is noted (straight arrow)

Imaging, surgical findings and pathology confirmed two cases associated with vascular invasion: one of them had tumor thrombus in the ipsilateral renal vein and the other had renal vein invasion and renal artery encasement with clear IVC (Table 4).

6 *Diffusion restriction*

Eighteen masses (72%) were found to be restricted in diffusion-weighted sequences (DWI) (Fig. 3 b). ADC values were measured in the restricted areas (Fig. 3 c). The region of interest (ROI) was fitted to area only intended to be measured to avoid averaging from surroundings. Its size averages 0.5 cm^2; however, in larger lesions; larger ROI size was used. ROI was fitted in a homogenous area and was measured in multiple sites in the restricted area, and the lowest mean value was taken. ADC values in the 18 restricted masses range from $0.5–1.4 \times 10^{-3}$ mm^2/s (diffusion restricted masses), and the mean ADC value was 0.88×10^{-3} mm^2/s. Seven masses (28%) showed free diffusion with higher ADC values more than 2×10^{-3} mm^2/s ranging from $2.0–2.5 \times 10^{-3}$ mm^2/s (diffusion-free masses).

Table 2 Distribution of lesions according to composition of the mass ($n = 25$)

Composition of the mass	No. of masses	Percentage
Cystic masses	3	12.0%
Renal abscess	1	4.0%
Xanthogranulomatous pyelonephritis	1	4.0%
Multiseptated cystic RCC	1	4.0%
Solid masses	11	44.0%
Clear cell RCC	2	8.0%
Papillary RCC	4	16.0%
Chromophobe RCC	2	8.0%
Oncocytoma	2	8.0%
Angiomyolipoma	1	4.0%
Solid masses with necrotic areas	11	44.0%
Clear cell RCC	6	24.0%
Papillary RCC	1	4.0%
Leiomyosarcoma	2	8.0%
Mixed papillary and clear cell RCC	1	4.0%
Carcinoma of collecting duct of Bellini	1	4.0%
Total	25	100.0%

Table 3 descriptive analysis of the studied masses according to presence of necrosis and intralesional hemorrhage (n = 25)

	MRI findings		Pathological findings		^{McN}p
	No	%	No	%	
Necrosis					
Negative (solid mass)	11	44.0%	12	48.0%	1.000
Positive necrosis	14	56.0%	13	52.0%	
Hemorrhage inside the mass					
Negative	18	72.0%	18	72.0%	1.000
Positive	7	28.0%	7	28.0%	

7 Discussion

Non-contrast MRI is a useful noninvasive imaging tool for diagnosis, characterization and differentiation of the most common types of renal masses in patients with renal impairment. It provides excellent soft tissue contrast and functional information. Renal MR imaging allows characterization of lesion location, extent, lymphovascular invasion and diffusion restriction and may allow differentiation of malignant from benign lesions. In addition, non-contrast MR imaging may aid in classifying RCC subtypes.

In our study, RCC was the most prevalent tumor subtype accounting for 90% of cases. This is similar to the reported data in the literature [4]. Regarding RCC subclassification, Ramamurthy et al. and Chivelle et al. stated that clear cell RCC is the most common subtype of RCC [7, 8]. Papillary carcinomas are the second most common subtype of RCC. They are bilateral in 4% of cases [8]. Chromophobe RRC is the third most common subtype [8]. This categorization coincides with the findings in our study.

Muglia et al., [9] reported that on T1-weighted images, clear cell RCC shows low to similar signal intensity when compared to that of the renal parenchyma. This comes in concordance with our results. Clear cell RCC seen in our patients showed iso- to hyperintense signal on T2w images, with hypo- to iso-intense signal on T1w images, and six out of eight clear cell RCC masses (75%) were heterogeneous showing central break down, which matches the literature stating that clear cell RCC tends to be heterogeneous with areas of necrosis [9, 10].

In our study, clear cell RCC masses with central break down showed central irregular area of T2-weighted

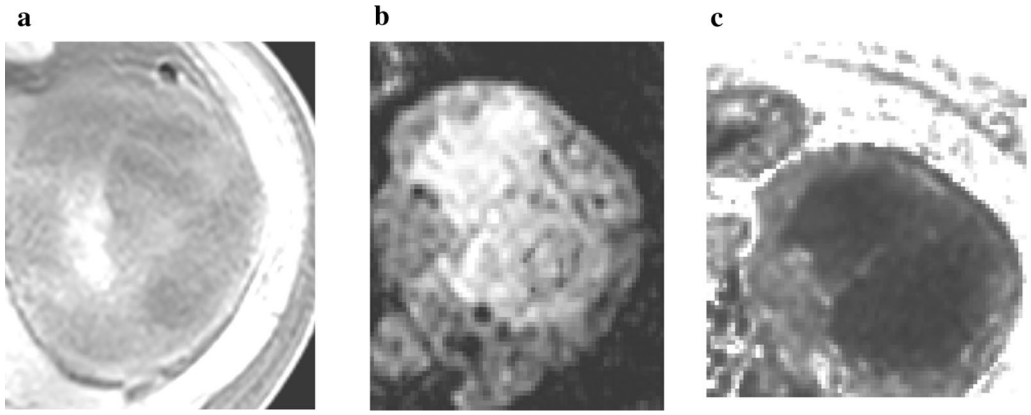

Fig. 3 Axial T1w image **a**, showing small hyperintense central area within the tumor representing central hemorrhagic area. Axial DW image **b** and the corresponding ADC image **c** showing areas of restricted diffusion within the tumor with the lowest ADC value 0.54×10^{-3} mm^2/s

Table 4 Descriptive analysis of the studied masses according to involvement of sinus fat, collecting system, perinephric fat, LN and vascular invasion

	MRI		Surgical findings		Pathological findings		Q	p
	No	%	No	%	No	%		
Renal sinus fat involvement (n = 25)								
Negative	17	68.0%	19	76.0%	20	80.0%	4.667	0.097
Positive	8	32.0%	6	24.0%	5	20.0%		
Collecting system involvement (n = 25)								
Negative	16	64.0%	18	72.0%	19	76.0%	3.500	0.174
Positive	9	36.0%	7	28.0%	6	24.0%		
Perinephric fat invasion (n = 25)								
Negative	17	68.0%	18	72.0%	18	72.0%	2.000	0.368
Positive	8	32.0%	7	28.0%	7	28.0%		
LN involvement (n = 20)								
Negative	14	70.0%	13	65.0%	13	65.0%	2.000	0.368
Positive	6	30.0%	7	35.0%	7	35.0%		
Vascular invasion (n = 20)								
Negative	18	90.0%	18	90.0%	18	90.0%	0.0	1.000
Positive	2	10.0%	2	10.0%	2	10.0%		

images hyperintensity and T1-weighted hypointensity. This coincides with what was stated by Gurel et al. that central necrosis is a homogeneous hypointense area in the center of the mass on T1-weighted images, with moderate to high signal intensity on T2-weighted images. Necrosis has been shown to correlate with tumor size and grade [10].

Some authors demonstrated that the smaller papillary RCCs are homogenous solid tumors, but when the tumor exceeds 4 cm in diameter, internal heterogeneity may be observed because of hemorrhage, calcification, and necrosis [9, 11]. This was not the case in all of the papillary RCC tumors included in our study, as we found one papillary RCC mass measured 7.7 cm in the largest dimension, still showed homogenous texture with no internal hemorrhage or necrotic changes. The other small papillary RCC masses measured less than 4 cm were all still homogenous lesions.

Vendrami et al. [12] stated that MR imaging features of papillary RCC in most cases show well-defined circumscribed homogenous peripherally located small sized (3 cm or less) tumors, with a surrounding fibrous capsule showing low signal intensity in both T1 and T2 weighted images. This is not matching with the finding in our study, as we encountered 5 papillary RCC masses, 3 of them showed the features stated by the literature, and the other 2 masses: one large sized (7.7 cm) homogenous mass with no internal hemorrhagic component and the other one was large sized mass (7 cm) with hemorrhagic content. No hypointense capsule was noted around any of the previously mentioned papillary RCC masses included in the study.

Intratumoral hemorrhage may occur and has a variable appearance depending on the stage of degradation of the blood products. Subacute to chronic hemorrhage generally demonstrates high signal intensity on both T1- and T2-weighted images, stated by Vendrami et al. [12]. This is comparable to the findings in our study, where renal masses with intralesional hemorrhagic contents showed T1 hyperintense signal with intermediate or low signal intensity on T2w images, so in our study, T1w sequence was the most important sequence for identifying intralesional hemorrhagic content [12].

Chromophobe RCC tends to be well-circumscribed and homogenous with no cystic changes or central necrosis even in large tumors; they show low to intermediate T2 signal intensity [9, 10]. This matches the MRI findings of the 2 cases of chromophobe RCC in our study; they were solid homogenous masses with intermediate T2 signal intensity.

There is consistent association between some MR imaging features and specific histological subtypes of RCC. Similarly, we found greater prevalence of high signal intensity on T2W images in patients with clear cell RCC, contrasting with lower signal intensity found in those with papillary RCC, chromophobe RCC [13–16].

Wang et al. [17] stated that RCC typically shows restricted diffusion, which is high signal intensity in DWI with corresponding low signal in ADC maps. These findings match the results obtained from the

current study where all cases of RCC showed restricted diffusion.

DWI can be helpful in detecting renal masses, especially in patients who cannot receive gadolinium contrast material. The presence of restricted diffusion and lower ADC values can be seen in masses that are both malignant and benign, including RCC, oncocytoma, AML, and renal abscess [12]. This matches with what we found in our results, as among the 20 malignant lesions encountered in our study, 16 (80%) masses showed areas of restricted diffusion and 4 (20%) masses demonstrated free diffusion (3 of them were papillary RCC and 1 clear cell RCC), and the benign tumors all showed free diffusion, while the 2 infective masses were restricted (XGPN and renal abscess). Based on these results, the presence of diffusion restriction cannot be considered a reliable feature for the malignant renal masses.

Regarding AML, our study showed that the gross macroscopic fat content appeared as T1 hyperintensity which was suppressed in the fat suppression sequence. Similarly Vendrami et al. [12] stated that classic AMLs (lipid-rich AML) demonstrate high T1 signal intensity because of the presence of macroscopic fat content. The presence of macroscopic fat can be appreciated as suppression of signal intensity on frequency-selective fat-saturated images [12].

Our results confirmed high correlation between non-contrast MRI findings and surgical/histopathological findings regarding perinephric, collecting system and vascular invasion. Additionally, lymph node involvement was closely correlated.

The use of non-contrast MRI in our study for this patient category proved many advantages. It has the best soft tissue contrast over CT and ultrasonography, which can make up for the absence of the contrast material administration and the value of mass enhancement, the detection of macroscopic fat by the frequency-selective fat-saturated images, the detection of microscopic fat by dropping signal in the opposed phase images, detection of fluid as high signal in T2 WI and detection of subacute hemorrhage or presence of protein rich content as high signal in T1 WI [18].

The limitations in our study were encountered in small sample size. Besides, the detection of the vascularity and pattern of enhancement of the masses, detection of small masses with signal intensity similar to that of the renal parenchyma and the differentiation between different RCC subtypes could not be significantly obtained in our study.

8 Conclusion

Recognition of the most important imaging features of solid renal masses may assist in their proper diagnosis and management. Non-contrast multiparametric MR imaging as a noninvasive imaging method provides critical information that can help in differentiation of the most common renal masses, including the common RCC subtypes and AMLs, and as a result may assist in selecting the most appropriate management and follow-up of these lesions.

Abbreviations

MRI: Magnetic resonant imaging; CT: Computerized tomography; RCC: Renal cell carcinoma; AML: Angiomyolipoma; ICM: Iodinized contrast material; CIN: Contrast-induced nephropathy; NSF: Nephrogenic systemic fibrosis; eGFR: Estimated glomerular filtration rate; TSE: T weighted sequence; DWI: Diffusion-weighted sequences; ADC: Apparent diffusion coefficient; ROI: Region of interest; XGPN: Xanthogranulomatous pyelonephritis.

Acknowledgements

Not applicable

Authors' contributions

OZ contributed to design of the work and data interpretation; RI contributed to data interpretation and drafting the work; RD contributed to data analysis and drafting the work; SG contributed to data acquisition and revision of the draft. All authors have approved the submitted version (and any substantially modified version that involves the author's contribution to the study). All authors have agreed both to be personally accountable for the author's own contributions and to ensure that questions related to the accuracy or integrity of any part of the work, even ones in which the author was not personally involved, are appropriately investigated, resolved, and the resolution documented in the literature. All authors read and approved the final manuscript.

Funding

None.

Availability of data and materials

Not applicable.

Declarations

Ethics approval and consent to participate

Verbal consent was obtained from all participants and was approved by the ethics committee. The medical ethics were considered including informed verbal consent that was obtained from all cases included in the study after explaining the purpose of the study. Confidentiality was maintained throughout the study. Institute: Faculty of medicine, University of Alexandria Ethical committee. Name of Ethical Committee members: Prof Dr Wael Nabeel and Prof Dr Ashraf Ettaby.

Consent for publication

Not Applicable.

Competing interests

None.

Author details

[1] Department of Urology, Faculty of Medicine, University of Alexandria, Alexandria, Egypt. [2] Department of Radiology, Faculty of Medicine, University of Alexandria, Alexandria, Egypt.

Received: 20 January 2021 Accepted: 29 March 2021
Published online: 09 April 2021

References

1. Volpe A, Panzarella T, Rendon RA, Haider MA, Kondylis FI, Jewett MA (2004) The natural history of incidentally detected small renal masses. Cancer 100(4):738–745
2. Cornelis F, Tricaud E, Lasserre AS et al (2014) Routinely performed multiparametric magnetic resonance imaging helps to differentiate common subtypes of renal tumours. Eur Radiol 24(5):1068
3. Allen BC, Tirman P, Jennings Clingan M, Manny J, Del Gaizo AJ, Leyendecker JR (2014) Characterizing solid renal neoplasms with MRI in adults. Abdom Imag 39(2):358–387
4. Motzer RJ, Agarwal N, Beard C et al (2011) Kidney cancer. J Natl Compr Canc Netw 9(9):960–977
5. Perez-Ordonez B, Hamed G, Campbell S et al (1997) Renal oncocytoma: a clinicopathologic study of 70 cases. Am J Surg Pathol 21(8):871–883
6. Pedrosa I, Sun MR, Spencer M, Genega EM, Olumi EF et al (2008) MR imaging of renal masses: correlation with findings at surgery and pathologic analysis. Radiographics 28:985–1003
7. Ramamurthy NK, Moosavi B, McInnes MD, Flood TA, Schieda N (2015) Multiparametric MRI of solid renal masses: pearlsand pitfalls. Clin Radiol 70(3):304–316
8. Cheville JC, Lohse CM, Zincke H, Weaver AL, Blute ML (2003) Comparisons of outcome and prognostic features among histologic subtypes of renal cell carcinoma. Am J SurgPathol 27:612–624
9. Muglia VF, Prando A (2015) Renal cell carcinoma: histologicalclassification and correlation with imaging findings. RadiolBras 48(3):166–174
10. Gurel S, Narra V, Elsayes KM, Siegel CL, Chen ZE, Brown JJ (2013) Subtypes of renal cell carcinoma: MRI and pathologicalfeatures. DiagnInterv Radiol 19(4):304–311
11. Prasad SR, Humphrey PA, Catena JR, Narra VR, Srigley JR, Cortez AD et al (2006) Common anduncommon histologic subtypes of renal cell carcinoma: imaging spectrum with pathologic correlation. Radio Graphics 26(6):1795–1806 (**discussion 1809-10**)
12. Vendrami CL, Villavicencio CP, Dejulio TJ, Chatterjee A, Casalino DD, Horowitz JM et al (2017) Differentiation of solid renal tumors with multiparametric MR imaging. Radiographics 37(7):2027–2042
13. Goyal A, Sharma R, Bhalla AS, Gamanagatti S, Seth A, Iyer VK et al (2012) Diffusion-weighted MRI in renal cell carcinoma: a surrogate marker for predicting nuclear grade and histological subtype. Acta Radiol 53(3):349–358
14. Pedrosa I, Chou MT, Ngo L, Baroni H, Genega R, Galaburda L et al (2007) MR classification of renal masses with pathologic correlation. Eur Radiol 18(2):365–75
15. Roy C, Sauer B, Lindner V, Lang H, Saussine C, Jacqmin D (2007) MR imaging of papillary renal neoplasms: potential application for characterization of small renal masses. EurRadiol 17(1):193–200
16. Morita S, Masukawa A, Suzuki K, Hirata M, Kojima S (2011) Unenhanced MR angiography: techniques and clinical applications in patients with chronic kidney disease. Radiographics 31:E13-33
17. Wang H, Cheng L, Zhang X, Wang D, Guo A, Gao Y et al (2010) Renal cell carcinoma: diffusion-weighted MR imaging for subtype differentiation at 3.0 T. Radiology 257(1):135–43
18. Kay FU, Canvasser NE, Xi Y, Pinho DF, Costa DN, Diaz de Leon A et al (2018) Diagnostic performance and interreader agreement of a standardized MR imaging approach in the prediction of small renal mass histology. Radiology 287(2):543–53

Publisher's Note